LAWRENCE
LIVERMORE
NATIONAL
LABORATORY

LLNL-JRNL-471000

Electrical Properties of Polycrystalline Methane Hydrate

W. L. Du Frane, L. A. Stern, K. A. Weitemeyer, S. Constable, J. C. Pinkston, J. J. Roberts

February 17, 2011

Geophysical Research Letters

Disclaimer

Electrical Properties of Polycrystalline Methane Hydrate

Wyatt L. Du Frane[1], Laura A. Stern[2], Karen A. Weitemeyer[3], Steven Constable[3], John C. Pinkston[2], Jeffery J. Roberts[1]

[1]Lawrence Livermore National Laboratory, 7000 East Ave, Livermore, CA 94551

[2]U. S. Geological Survey, 345 Middlefield Rd, MS/977, Menlo Park, CA 94025

[3]Scripps Institution of Oceanography, 8800 Biological Grade, La Jolla, CA 92093

Electromagnetic (EM) remote-sensing techniques are demonstrated to be sensitive to gas hydrate concentration and distribution and complement other resource assessment techniques, particularly seismic methods. To fully utilize EM results requires knowledge of the electrical properties of individual phases and mixing relations, yet little is known about the electrical properties of gas hydrates. We developed a pressure cell to synthesize gas hydrate while simultaneously measuring *in situ* frequency-dependent electrical conductivity (σ). Synthesis of methane (CH_4) hydrate was verified by thermal monitoring and by post run cryogenic scanning electron microscope imaging. Impedance spectra (20 Hz to 2 MHz) were collected before and after synthesis of polycrystalline CH_4 hydrate from polycrystalline ice and used to calculate σ. We determined the σ of CH_4 hydrate to be 5 x 10^{-5} S/m at 0 °C with activation energy (E_a) of 30.6 kJ/mol (-15 to 15 °C). After dissociation back into ice, σ measurements of samples increased by a factor of ~4 and E_a increased by ~50%, similar to the starting ice samples.

1. Introduction

Clathrate hydrates of natural gas are compounds with an ice-like crystalline framework that encages guest gas molecules, most commonly methane (CH_4). CH_4 hydrate formation requires cool temperature, high pressure, and sufficient supplies of H_2O and CH_4; these conditions are met in both marine and permafrost regions worldwide [*Kvenvolden*, 1999]. CH_4 hydrate is potentially a significant source of clean, low-carbon energy. However, some naturally occurring hydrate in the arctic exists at the edge of thermodynamic stability posing an environmental hazard that threatens release of potent greenhouse gases [e.g., *Shakhova et al.*, 2010], and posing a more local and immediate threat to drilling and wellbore stability [*Dawe and Thomas*, 2007].

CH_4 hydrate occurs in vast quantities, with an estimate of 10,000 Gt of CH_4 as the highly cited 'consensus value' [*Kvenvolden*, 1999; *Milkov*, 2004]; however, other estimates span several orders of magnitude as a result of continued efforts at direct and indirect observation and by the addition of more complex global models [e.g., *Boswell and Collett*, 2010; *Maslin et al.*, 2010]. Current geophysical surveying methods for identifying hydrate are limited. Well logging or coring is expensive, invasive, and provides only a point measurement for the direct presence of hydrate. Seismic methods detect hydrate using seismic bottom simulating reflectors, blanking, and bright spots [e.g., *Hornbach et al.*, 2003]. Quantifying the volume fraction of hydrate in sediments may be possible with careful processing and inversion of seismic data [e.g., *Hornbach et al.*, 2003; *Zhang and McMechan*, 2006], but this approach is complicated.

Well logging indicates that regions containing hydrate are significantly less conductive than water saturated zones [e.g., *Collett and Ladd*, 2000]. This is consistent with the demonstrated sensitivity of electromagnetic (EM) methods to the concentration and geometric distribution of hydrate and pore fluid [*Edwards*, 1997; *Evans*, 2007; *Schwalenberg et al.*, 2005; *Weitemeyer et al.*, 2006a; 2006b]. However, to make quantitative estimates of hydrate volume using EM methods requires knowledge of the electrical conductivity (σ) of gas hydrates in combination with petrophysical mixing relations, particularly in cases of highly saturated gas hydrate with only minor, poorly connected, pore water.

To date, there have been few published measurements on the electrical properties of sediment-gas hydrate-water mixtures and none on unmixed, single-phase CH_4 hydrate. *Spangenberg and Kulenkampff* [2006] examined the σ of glass beads as a function of CH_4 hydrate saturation in the pore space at ~13 °C. *Lee et al.* [2010] published a systematic examination of σ and permittivity of tetrahydrofuran hydrate (an analog for natural gas hydrate)

mixed with sand, silts, and clay at ~0 °C. Ren et al. [2010] studied a mixture of sand, CH_4 hydrate, and seawater from 5-30 °C, however temperature was not controlled independently of CH_4 hydrate saturation. Studies on mixed samples help to resolve mixing laws, but the σ of these samples are dominated by the water and/or sediment, with no quantitative information on the σ of the gas hydrate. In this study we present the first σ measurements on unmixed CH_4 hydrate over a large temperature range that encompasses that of natural hydrate formations.

2. Experimental Techniques

We designed a specialty pressure cell to form polycrystalline CH_4 hydrate for *in situ* impedance (Z) measurements (Figure 1). An Agilent E4980A LCR (inductance-capacitance-resistance) meter was used to measure complex Z spectra between 20 Hz to 2 MHz with a relative accuracy 0.01% degrading to 1% for Z of 10 MΩ. The assembly was tested for electrical leakage using a blank sample made of Teflon, ice frozen from reagent grade water, and a variety of parallel resistor-capacitor (R-C) circuits (10-316 kΩ; 1.15-22 pF). We performed 3 runs with CH_4 hydrate: run 1 with a thermocouple installed in the cell to verify the synthesis process and extent of reaction, and then runs 2 and 3 to measure σ. Samples of CH_4 hydrate were synthesized from a granular ice + CH_4 gas mixture at 25 +/- 5 MPa using a temperature cycling method described previously in *Stern et al.* [1996; 2004]. The reactant ice was made from a block of nearly gas-free ice grown from distilled-deionized water, then crushed and sieved to 180-250 μm. We measured Z and σ in runs 2 and 3 during the first heating cycle, after full reaction to CH_4 hydrate, and after samples were dissociated back into polycrystalline ice. Heating was isochoric such that the pore pressure of CH_4 gas increased during the measurement (pressure ranges are listed in Table 1). While heating or cooling, temperature in the center of the run 1 sample lagged slightly behind bath temperature by 1-5°C, leading to slight uncertainty in sample

69 temperature during heating for runs 2 and 3. We addressed this in run 3 by monitoring Z at a
70 single frequency after each heating increment and recording σ after it stopped changing. In Table
71 1 this is called 'step-dwell'.
72 Cryogenic scanning electron microscopy (cryo-SEM) was used to observe the grain size
73 and appearance of the final CH_4 hydrate formed in run 1. For this procedure, the vessel was
74 cooled sufficiently with liquid nitrogen prior to depressurization and opening of the cell. A
75 thermocouple embedded in the sample was used to ensure stability of the hydrate during the
76 quenching procedure, recovery, and transfer to the cryo-preparation station (Gatan Alto Model
77 2100). The sample was cleaved under vacuum in the preparation station to produce fresh
78 surfaces uncontaminated by water condensation, and then transferred under vacuum to a
79 LEO982 field emission SEM. A thermocouple embedded in the SEM sample stage monitored
80 temperature throughout the imaging process. Imaging was conducted at temperature < 102 K,
81 vacuum < 10^{-6} kPa, and accelerating voltage of 2 kV. Further details are given in *Stern et al.*
82 [2004].
83 **3. Results**
84 Cryo-SEM images of the crystal morphology and thermal monitoring of run 1 confirmed
85 the synthesis of CH_4 hydrate (Figure 2). The resulting polycrystalline material has 20 – 70 μm
86 average grain diameters and ~ 20% intergranular porosity. The porosity is also known
87 independently from mass measurements of the reactant ice prior to loading the cell. Most of the
88 porosity occurs as isolated and virtually unconnected cavities (Fig. 2a), and so will have minimal
89 effect on σ. Ice was not observed in the interior of the sample.
90 Plots of complex Z from runs 2 and 3 consist of two overlapping, semicircular arcs
91 (Figure 3a). The silver foil electrodes were polarizing and did not allow transfer of charge from

92 the samples (i.e., 'blocking'), resulting in large low frequency arcs (shown partially in Figure
93 3a). We attribute the smaller, high frequency arcs to sample properties [*Roberts and Tyburczy*,
94 1993]. Z spectra were fit with an equivalent circuit of two R-Cs in series [*Roberts and Tyburczy*,
95 1991], which demonstrated that σ could be reliably measured with the frequency associated with
96 the smallest phase angle to eliminate electrical response related to the vessel, leads or electrodes
97 (Figure 3a).

98 For runs 2 and 3, σ was measured during the initial heating cycle and after CH_4 hydrate
99 was fully synthesized (i.e. after $\geq$ 6 heating cycles). The samples were then dissociated to
100 polycrystalline ice by venting the pressurized CH_4 from the sample at -15 °C (1 day for run 2,
101 and 13 days for run 3). In both runs, σ of the samples as CH_4 hydrate were a factor of ~3-4 lower
102 than σ of the samples as ice. For both ice and CH_4 hydrate, σ exhibited typical Arrhenius
103 behavior (Figure 3b). Therefore, we fit the σ data as a function of absolute temperature (T) using

104 $$\sigma(T) = \sigma_0 e^{-Ea/(RT)} \quad (1)$$

105 where σ_0 is a pre-exponential constant corresponding to $T = \infty$, E_a is activation energy, and R is
106 the gas constant (fitting results listed in Table 1). Larger error is associated with E_a calculated
107 during active heating, because of the variable amount by which the bath temperature lagged
108 sample temperature. We consider the E_a calculated from run 3 using the 'step-dwell' approach to
109 be the more reliable, nevertheless there is good agreement between runs 2 and 3 (Figure 3b).

110 **4. Discussion**

111 Previous experience indicates that most sample transformation to hydrate occurs while
112 passing the melting point of ice during the first heating cycle [*Stern et al.*, 2004]. Our σ results
113 during the first cycle are consistent with this, assuming that ice dominated the electrical

114 properties of the sample below its melting point, and the small amount of unreacted liquid water
115 dominated above the ice point (Figure 3b).
116 After several more heating/cooling cycles we do not observe a discontinuity in σ or E_a
117 below or above the melting point of ice, suggesting that samples had fully reacted into CH_4
118 hydrate. This is consistent with previous observations that all ice reacts within 1-5
119 heating/cooling cycles, depending in part on the on the grain size and packing density of the
120 initial ice grains [*Stern et al.*, 1996; 2004]. In both runs 2 and 3, synthesis of CH_4 hydrate
121 resulted in lower σ and E_a in our samples compared to the first heating cycle. Using the Hashin-
122 Shtrikman mixing model we calculate that σ of nonporous CH_4 hydrate would be a factor of 1.37
123 (0.137 log units) higher than our measurements for 20% porous gas hydrate.
124 After venting the samples, most of the CH_4 hydrate dissociated to ice within several
125 hours; however, the dissociation rates for the last remaining hydrate is complicated by the effects
126 of self preservation or self buffering of the hydrate [*Stern et al.*, 2001]. For run 2 a small amount
127 of hydrate may have remained in the samples at the center of grains, in which case this secondary
128 phase would be poorly connected and have little contribution to the measured electrical
129 properties. Run 3 dissociated for a much longer period and likely had no hydrate remaining in
130 the sample when σ was measured. In both runs σ and E_a were lower for CH_4 hydrate than for the
131 dissociated ice product.
132 The σ of ice is known to be determined by the concentration of intrinsic Bjerrum defects
133 (L and D) and extrinsic protonic defects (H_3O^+ and OH^-) resulting from ionic impurities, with
134 higher concentrations/mobilities of these defects in grain surfaces than in the bulk grains [e.g.,
135 *Petrenko and Whitworth*, 1999]. Assuming similar defects conduct charge in hydrate suggests
136 the magnitude of σ is also likely to be dependent on impurities. Although we did not characterize

137 the impurity of our samples, the same ionic impurities existed in the bulk samples as either ice or
138 hydrate. Good reproducibility of σ measurements suggests similar concentrations of impurities
139 were in samples from runs 2 and 3.

140 Lower σ in hydrate than ice is consistent with greater site spacing. Accommodation of a
141 large hydrocarbon molecule in the clathrate structure potentially reduces the site densities of all
142 point defects relative to the ice structure (I_h) which would increase the energy necessary for
143 defects to hop to neighboring sites. This would result in reduced defect mobilities and may
144 explain why both σ (this study) and thermal conductivity [*deMartin*, 2001; *Waite et al.*, 2007] are
145 lower for hydrate than ice.

146 **5. Conclusion**

147 We have performed the first electrical measurements of unmixed, polycrystalline CH_4
148 hydrate (with ~ 20% unconnected intergranular porosity), over the temperature range of -15 to 15
149 °C; the E_a is 30.6 kJ/mol. We measure σ of CH_4 hydrate at 0 °C to be 5×10^{-5} S/m, which helps
150 to verify that EM surveys may be used to map hydrates in seafloor sediments and provides a
151 more quantitative basis for modeling using mixing laws. Future experiments will be conducted
152 on CH_4 hydrate + sediment aggregates (± seawater) to measure electrical properties of mixed-
153 phase samples.

154 **Acknowledgements**

155 The authors thank W. Durham (MIT) and D. Lockner, W. Waite, and S. Kirby (USGS)
156 for helpful discussions and advice, and J. Lemire (SIO) for help with the cell fabrication and
157 design. We also thank R. Evans (WHOI) and another anonymous reviewer. Support for this work
158 was provided by DOE contract, DE-NT0005668. Prepared by LLNL under Contract DE-AC52-
159 07NA27344.

References

Boswell, R., and T. Collett (2010), Current perspectives on gas hydrate resources, *Energy Environ. Sci.*, doi: 10.1039/C0EE00203H.

Collett, T. S., and J. W. Ladd (2000), Detection of gas hydrate with downhole logs and assessment of gas hydrate concentrations (saturations) and gas volumes on the Blake Ridge with electrical resistivity log data, *Proc. Ocean Drill. Program, Sci. Results*, *164*, 179-191.

Dawe, R. A., and S. Thomas (2007), A large potential methane source - Natural gas hydrates, *Energy Sources Part A-Recovery Util. Environ. Eff.*, *29*(3), 217-229.

deMartin, B. J. (2001), Laboratory measurement of the thermal conductivity and thermal diffusivity of methane hydrate at simulated in-situ conditions, M.S. Thesis, Sch. Earth Atmos. Sci., Georgia Inst. Tech., Atlanta, GA.

Edwards, R. N. (1997), On the resource evaluation of marine gas hydrate deposits using sea-floor transient electric dipole-dipole methods, *Geophysics*, *62*(1), 63-74.

Evans, R. L. (2007), Using CSEM techniques to map the shallow section of seafloor: From the coastline to the edges of the continental slope, *Geophysics*, *72*(2), WA105-WA116.

Hornbach, M. J., W. S. Holbrook, A. R. Gorman, K. L. Hackwith, D. Lizarralde, and I. Pecher (2003), Direct seismic detection of methane hydrate on the Blake Ridge, *Geophysics*, *68*(1), 92-100.

Kvenvolden, K. A. (1999), Potential effects of gas hydrate on human welfare, *Proc. Natl. Acad. Sci. U. S. A.*, *96*(7), 3420-3426.

Lee, J. Y., J. C. Santamarina, and C. Ruppel (2010), Parametric study of the physical properties of hydrate-bearing sand, silt, and clay sediments: 1. Electromagnetic properties, *J. Geophys. Res., [Solid Earth]*, *115*: B11104, doi:10.1029/2009JB006669.

183 Maslin, M., M. Owen, R. Betts, S. Day, T. Dunkley Jones, and A. Ridgwell (2010), Gas
184 hydrates: past and future geohazard?, *Proc. R. Soc. A, 368*(1919), 2369-2393.
185 Milkov, A. V. (2004), Global estimates of hydrate-bound gas in marine sediments: how much is
186 really out there?, *Earth-Sci. Rev.*, *66*(3-4), 183-197.
187 Petrenko, V. F., and R. W. Whitworth (1999), *Physics of Ice*, Oxford Univ. Press Inc., New
188 York.
189 Ren, S. R., Y. Liu, and W. Zhang (2010), Acoustic velocity and electrical resistance of hydrate
190 bearing sediments, *J. Petrol. Sci. Eng.*, 70, 52-56.
191 Roberts, J. J., and J. A. Tyburczy (1991), Frequency-dependent electrical-properties of
192 polycrystalline olivine compacts, *J. Geophys. Res., [Solid Earth]*, *96*(B10), 16205-16222.
193 Roberts, J. J., and J. A. Tyburczy (1993), Impedance spectroscopy of single and polycrystalline
194 olivine - evidence for grain-boundary transport, *Phys. Chem. Miner.*, *20*(1), 19-26.
195 Schwalenberg, K., E. Willoughby, R. Mir, and R. N. Edwards (2005), Marine gas hydrate
196 electromagnetic signatures in Cascadia and their correlation with seismic blank zones, *First*
197 *Break*, *23*, 57-63.
198 Shakhova, N., I. Semiletov, A. Salyuk, V. Yusupov, D. Kosmach, and O. Gustafsson (2010),
199 Extensive Methane Venting to the Atmosphere from Sediments of the East Siberian Arctic
200 Shelf, *Science, 327*(5970), 1246-1250.
201 Spangenberg, E., and J. Kulenkampff (2006), Influence of methane hydrate content on electrical
202 sediment properties, *Geophys. Res. Lett.*, *33*(24).
203 Stern, L. A., S. Circone, S. H. Kirby, and W. B. Durham (2001), Anomalous preservation of pure
204 methane hydrate at 1 atm, *J. Phys. Chem. B, 105*(9), 1756-1762.

Stern, L. A., S. H. Kirby, and W. B. Durham (1996), Peculiarities of methane clathrate hydrate formation and solid-state deformation, including possible superheating of water ice, *Science*, *273*(5283), 1843-1848.

Stern, L. A., S. H. Kirby, S. Circone, and W. B. Durham (2004), Scanning electron microscopy investigations of laboratory-grown gas clathrate hydrates formed from melting ice, and comparison to natural hydrates, *Am. Mineral.*, *89*(8-9), 1162-1175.

Waite, W. F., L. A. Stern, S. H. Kirby, W. J. Winters, and D. H. Mason (2007), Simultaneous determination of thermal conductivity, thermal diffusivity and specific heat in sI methane hydrate, *Geophysical J. Int.*, *169*(2), 767-774.

Weitemeyer, K. A., S. C. Constable, and K. W. Key (2006a), Marine EM techniques for gas-hydrate detection and hazard mitigation, *The Leading Edge*, *25*, 629-632.

Weitemeyer, K. A., S. C. Constable, K. W. Key, and J. P. Behrens (2006b), First results from a marine controlled-source electromagnetic survey to detect gas hydrates offshore Oregon, *Geophys. Res. Lett.*, *33*(3).

Zhang, Z. J., and G. A. McMechan (2006), Elastic inversion for distribution of gas hydrate, with emphasis on structural controls, *J. Seismic Explor.*, *14*(4), 349-370.

Table 1. Summary of experimental conditions and Equation 1 fit parameters for σ_0 and E_a.

Run	Sample condition	Heating Cycle	Heating Rate (°C/hr)	CH_4 Pore Pressure (MPa)	Log(σ_0 (S/m))	E_a (kJ/mol)
1	Synthesis Test	n/a	6.2	16.9-25.8[†]	n/a	n/a
2	Ice w/ CH_4	1	7.4	21.7-26.2	1.16[*]	25.8[*]
	CH_4 hydrate	11	5.9	18.3-21.3	0.965	27.9
	Dissociated to ice	12	4.7	0	6.63[*]	54.5[*]
3	Ice w/ CH_4	1	9.8	23.0-26.7	0.376[*]	21.8[*]
	CH_4 hydrate	7	Step-Dwell	16.2-18.5	1.50	30.6
	Dissociated to ice	8	Step-Dwell	0	5.00[*]	45.3[*]

[†]Pressure range over entire run.

[*]Fits only include data below ice melting point.

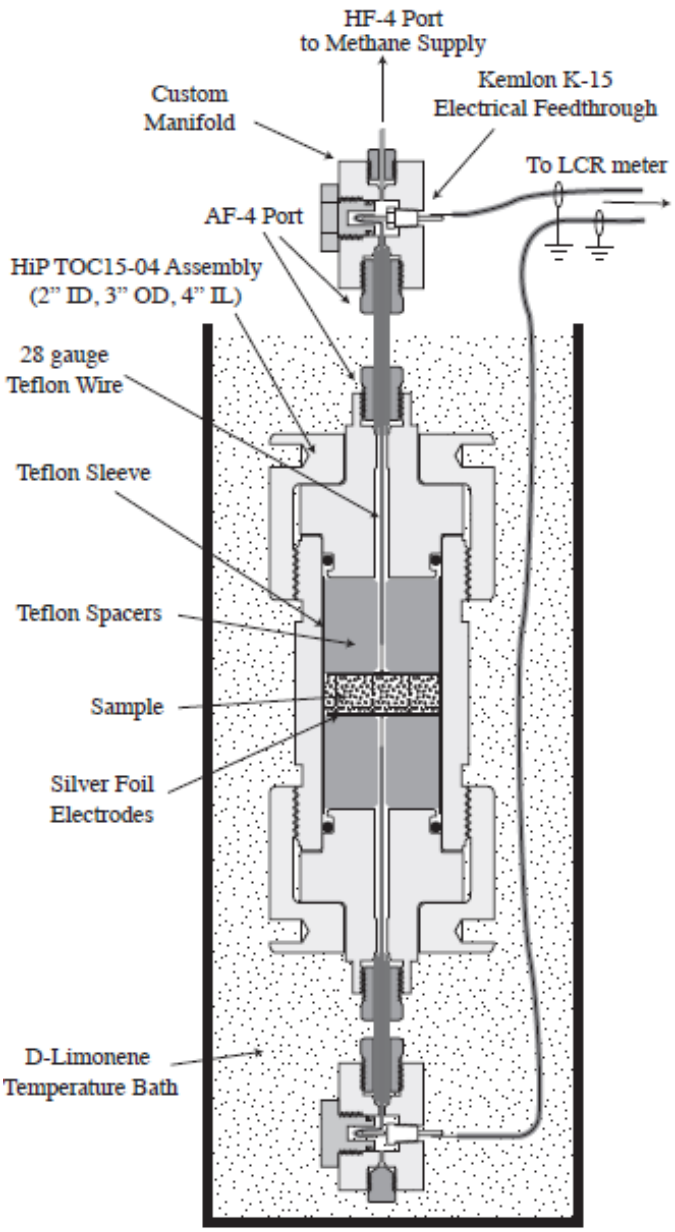

224

225 **Figure 1.** Schematic of σ cell, built around a commercially available double-ended pressure
226 vessel manufactured by High Pressure Equipment Co. with a pressure rating of 5,000 psi (34.5
227 MPa). Silver foil electrodes are connected by Teflon insulated wire to high pressure electrical
228 feedthroughs (Kemlon brand K-15) on the inner (high pressure) side and the Agilent E4980A
229 LCR meter on the outer side. The cell encloses a 5 x 1.25-cm disc-shaped sample, with
230 electrodes at each end and capped by Teflon spacers and surrounded by a Teflon sleeve.

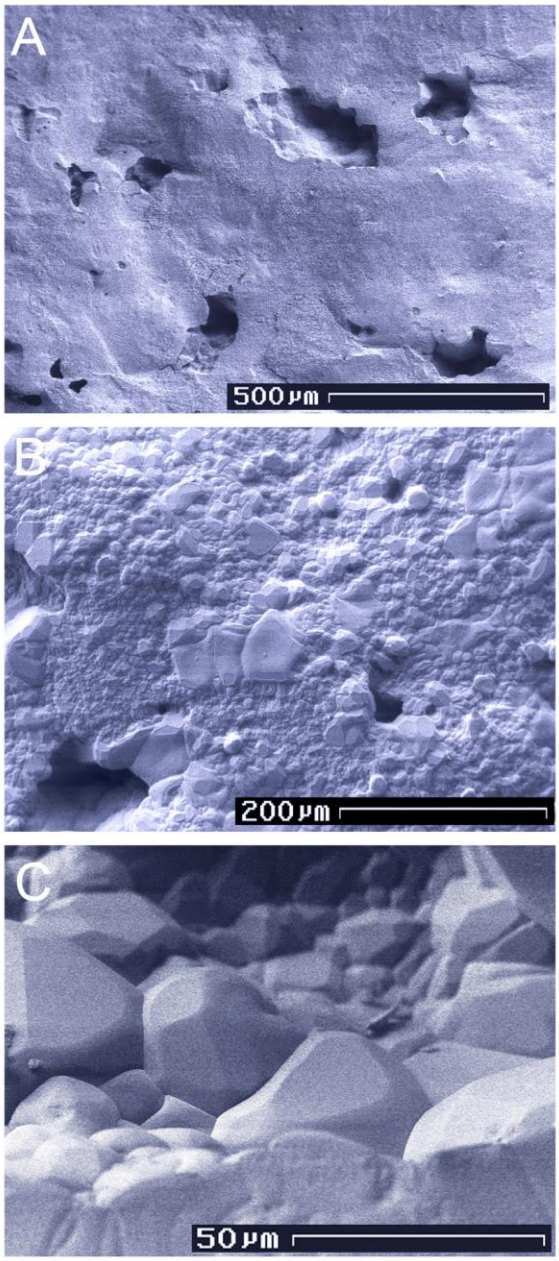

Figure 2: Cryo-SEM images of CH_4 hydrate formed in run 1, showing overall sample appearance (A) and closer views of individual grains (B, C).

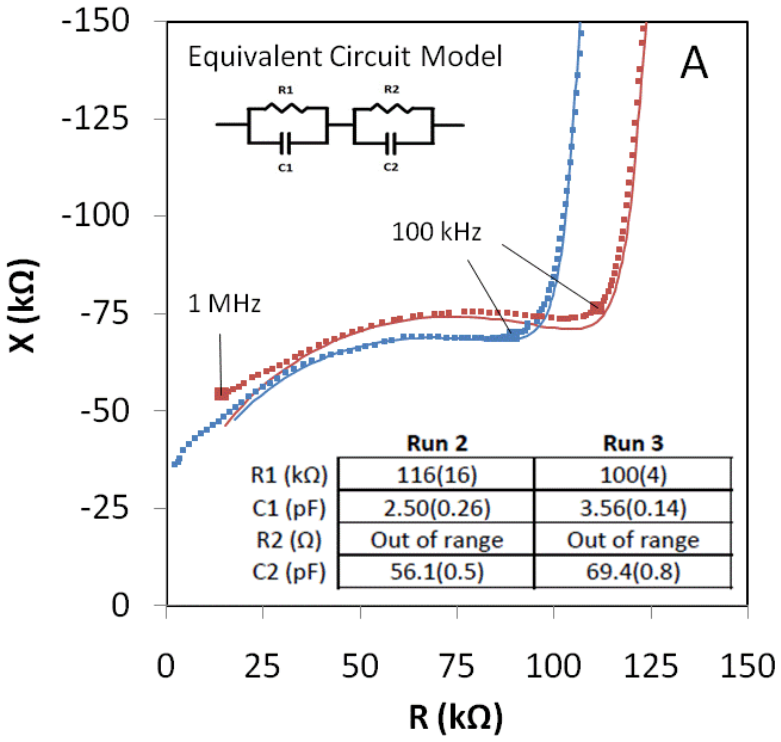
Equivalent Circuit Model
R1
R2
C1
C2
A
100 kHz
1 MHz
X (kΩ)
R (kΩ)
-150
-125
-100
-75
-50
-25
0
0
25
50
75
100
125
150
Run 2
Run 3
R1 (kΩ) 116(16) 100(4)
C1 (pF) 2.50(0.26) 3.56(0.14)
R2 (Ω) Out of range Out of range
C2 (pF) 56.1(0.5) 69.4(0.8)

235

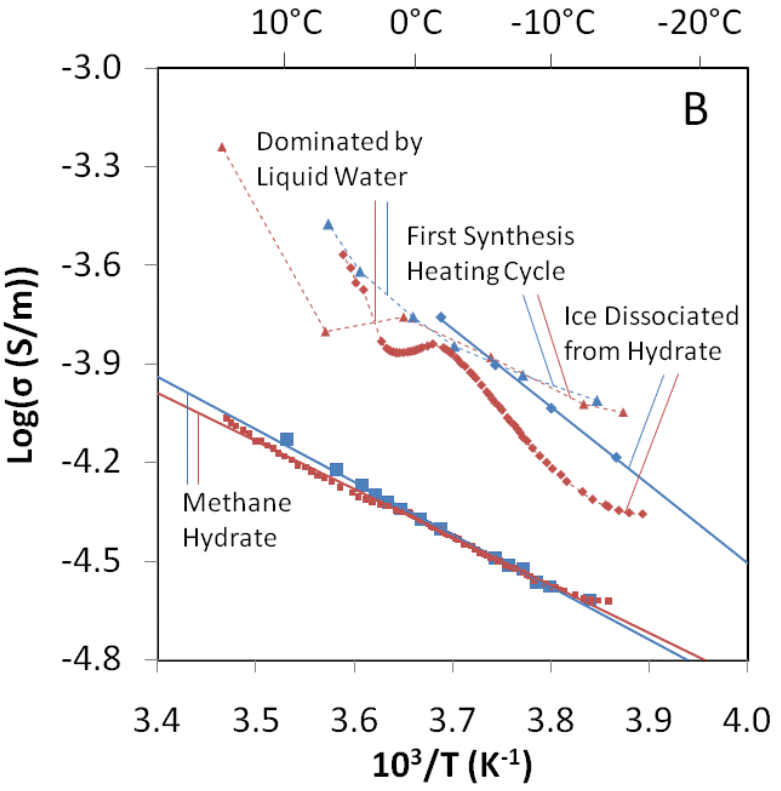
10°C
0°C
-10°C
-20°C
B
Dominated by
Liquid Water
First Synthesis
Heating Cycle
Ice Dissociated
from Hydrate
Methane
Hydrate
Log(σ (S/m))
-3.0
-3.3
-3.6
-3.9
-4.2
-4.5
-4.8
3.4
3.5
3.6
3.7
3.8
3.9
4.0
10³/T (K⁻¹)

236

Figure 3. Z and σ measurements from runs 2 (red) and 3 (blue) with data fits shown as solid lines (corresponding colors). 3a) shows complex Z spectra of polycrystalline CH_4 hydrate from runs 2 and 3 at 4°C, modeled with two parallel R-C pairs in series. Real Z ($R = Z*\cos(\theta)$) is plotted vs. imaginary Z ($X = Z \sin(\theta)$), where $|Z|^2 = R^2 + X^2$ and $\theta = \tan^{-1}(X/R)$. Fitting results are given in lower inset, with errors provided in parentheses. Z spectra consist of overlapping semicircular arcs. The smaller arcs at high frequency ($\geq$ ~100 kHz at 4 °C) resulted from the material properties of the samples (R1, C1). The larger arcs at low frequency (shown partly as a rapid change in X for R > ~100 kΩ and frequencies $\leq$ ~100 kHz at 4 °C) were caused by electrode polarization (R2, C2). Modeling indicates that σ can be calculated from |Z| corresponding to the smallest value of |θ|. 3b) σ collected during the first heating cycle (triangles), after methane hydrate synthesis (squares), and after dissociation to ice (diamonds). CH_4 hydrate is ~0.6 log units below ice, and has ~33% lower E_a (proportional to the slope of data fits, results in Table 1).